Springer

Acta Mechanica Sinica

CrossMark click for updates

• RESEARCH PAPER •

Acta Mech. Sin., Vol. 40, 523428 (2024)
https://doi.org/10.1007/s10409-023-23428-x

Ultra-chaos of square thin plate in low Earth orbit

Bo Zhang, Yu Yang, and Shijun Liao*

School of Naval Architecture, Ocean and Civil Engineering, Shanghai Jiao Tong University, Shanghai 200240, China

Received October 20, 2023; accepted November 28, 2023; published online May 28, 2024

Due to its small mass and eccentricity, the motion of a piece of debris in low Earth orbit (LEO) may be chaotic. This paper demonstrates that ultra-chaos widely exists in the case of a square thin plate in LEO with a center of mass (COM) that is initially displaced from the axis of symmetry. Chaotic systems are well-known for their sensitive dependence on initial conditions, though their statistical properties are usually insensitive to small disturbances. However, a recent concept called ultra-chaos has been introduced to describe chaotic systems whose statistics are sensitive to even tiny disturbances. This paper demonstrates that ultra-chaos is widely exists in a square thin plate in LEO with a displaced COM from the axis of symmetry. The results show that an ultra-chaotic plate trajectory exhibits higher disorder than that of a normal plate, with a position deviation that can be two orders of magnitude larger than that of a normal-chaotic subsystem. Distinct from earlier findings concerning ultra-chaotic systems, the present study uncovers the manifestation of ultra-chaos in a physically constrained system devoid of periodic boundaries. Prior investigations of ultra-chaotic systems have featured at least one periodic boundary or lacked a physical boundary. The new concept of ultra chaos provides a plausible explanation as to why space debris can spread to a vast area, as most pieces of debris have a displaced COM.

Chaos, Numerical simulation, Low Earth orbit

Citation: B. Zhang, Y. Yang, and S. Liao, Ultra-chaos of square thin plate in low Earth orbit, Acta Mech. Sin. **40**, 523428 (2024), https://doi.org/10.1007/s10409-023-23428-x

1. Introduction

Space debris does great harm to in-orbit satellites. The number of cataloged objects increased almost exponentially, and there are at least 19,477 pieces of debris in low Earth orbit (LEO) [1]. These debris comes from launch operations and anti-satellite (ASAT) tests. A serious consequence of ASAT is that the resulting debris cloud remains very stable for quite a long time [2-4]. Accurate prediction of the trajectory of space debris has become increasingly important regarding the safety of in-orbit satellites. The predictions of trajectories of space objects before reentry are generally divided into three categories: short-term, medium-term, and long-term [5]. Medium and long-term predictions are used to monitor the debris over periods ranging from a few weeks to several years, and over the short-term in the final few days before reentry, which usually occurs at orbit altitudes below 200 km. Unfortunately, forecasting the trajectories of space objects is an intractable problem primarily because the motion of debris objects is mostly chaotic [6] given that their trajectories possess sensitivity dependence on initial condition (SDIC), called "butterfly-effect" [7], so that long-term prediction of chaos is impossible. The SDIC corresponds to the trajectory instability of chaos [8, 9].

Chaos exists widely in the dynamical systems of space objects. Celletti et al. [10] discussed the phenomenon of overlapping of orbital resonances, and the chaotic motion of space debris caused by the effect of large area-to-mass ratio and the influence of lunisolar secular resonances. As pointed out by Daquin et al. [11], the chaotic motion of global navigation satellite systems is caused by orbital resonances. Aslanov [12] found that space debris with tethered tow has

*Corresponding author. E-mail address: sjliao@sjtu.edu.cn (Shijun Liao)

Executive Editor: Lifeng Wang

© The Chinese Society of Theoretical and Applied Mechanics and Springer-Verlag GmbH Germany, part of Springer Nature 2024

chaotic behavior, which is influenced by the damping ratio of the tether. Serra et al. [13] investigated different objects by means of numerical integration of a high precision model and found that the quaternions of the plate exhibit chaotic behavior. Khan et al. [14] studied the chaotic properties of the angular velocity of a satellite exposed to a set of prescribed external forces. Aslanov et al. [15] reported that a small eccentricity can make the attitude of the re-entry capsule chaotic, and with that small eccentricity, a gentle wind or a change in the mass distribution of the object will destroy the forecast. All the foregoing examples support the finding that the trajectories of space objects inkling space debris are mostly chaotic.

Lorenz [16,17] was the first to discover that chaotic trajectories exhibit sensitivity dependence on the conventional numerical algorithms, time-step, etc. Unfortunately, unlike initial conditions, the conventional numerical algorithms, time-step, etc., are artificial and so have no physical meaning. Obviously, a true physical solution must be completely independent of these artificial factors, and this has led to intense debate on the on the reliability and convergence of numerical simulations of chaotic systems [18-31]. Why is this the case? Numerical noise caused by truncation and round-off errors are unavoidable in any numerical simulation.

Why? Note that numerical noises caused by truncation error and round-off error are unavoidable in any numerical simulations. Thus, due to the butterfly-effect, the false numerical error from a computer-generated simulation $\mathcal{S}'$ of a chaotic system increases exponentially, so that it quickly becomes a mixture of the true physical solution $\mathcal{P}$ and false numerical noise δ', which are mostly of the same order of magnitude, i.e., $\delta' \sim \mathcal{P} \sim \mathcal{S}'$. Despite this, such kind of badly polluted result $\mathcal{S}'$ are widely used to calculate statistical results, because it is widely accepted by the scientific community that statistical results based on the "dirty" simulation $\mathcal{S}' = \mathcal{P} + \delta'$ (i.e., a mixture of $\mathcal{P}$ and δ') should be the same as those given by the true physical solution $\mathcal{P}$, say

$$\langle \mathcal{P} + \delta' \rangle = \langle \mathcal{P} \rangle, \qquad \text{when } \delta' \sim \mathcal{P} \text{ mostly}, \tag{1}$$

where $\langle\rangle$ denotes a statistical operator. Unfortunately, this is only a hypothesis for chaotic systems, since there was no way to separate the true physical solution $\mathcal{P}$ from the badly polluted simulation $\mathcal{S}'$ until 2009 when Liao [32, 33] proposed clean numerical simulation (CNS) [34-40]. Unlike conventional numerical algorithms in single (or double) precision floating-point arithmetic, CNS can obtain the convergent trajectory $\mathcal{S}$ of chaos in a prescribed sufficiently long time interval $t \in [0, T_c]$, where T_c is called the "critical predictable time", during which the false numerical noise δ' is of much lower order of amplitude than the true physical solution, i.e., $|\delta'| \ll |\mathcal{S}|$ so that the chaotic simulation $\mathcal{S}$ given by CNS is a very accurate approximation of the true physical solution $\mathcal{P}$, say, $\mathcal{S} \approx \mathcal{P}$. Therefore, for the first time, CNS has provided us with the ability to check the statistics stability of chaotic systems, i.e., the hypothesis (1), in which $\mathcal{P} + \delta'$ is given by conventional algorithms in single (or double) precision, and $\mathcal{P}$ is accurately obtained by CNS, separately. Using CNS as a powerful tool, it was discovered that many chaotic systems have statistics instability [35, 36], such that the hypothesis does not always hold. This surprising fact leads to a completely new concept of "ultra-chaos" [37] and a completely new classification of chaos into "normal-chaos" whose statistics are stable to small disturbances, and "ultra-chaos" whose statistics are unstable. It has been found that ultra-chaos widely exists in chaotic systems [38, 39]. It is important to distinguish between "ultra-chaos" and "hyper-chaos" in the context of chaotic systems. The latter refers to a concept used to characterize the chaotic behavior of a system exhibiting multiple positive Lyapunov exponents. Conversely, "ultra-chaos" is a term introduced by Liao and Qin [37] to denote the chaotic behavior of a system that demonstrates statistical instability when subjected to minor disturbances. In fact, it has been determined that the well-known hyper-chaotic Rossler system exhibits behavior consistent with normal chaos [37]. This study aims to provide fundamental insight into the chaotic properties of the finite-dimensional debris system in the LEO. The objective is to investigate how different types of chaos influence the prediction of debris trajectories. The outline of the present study is as follows: Section 2 describes the geometric model, the motion equations, and the numerical method. Section 3 describes the fundamental differences between ultra-chaos and normal-chaos, and their influences on the debris system. Section 4 presents the conclusions and gives a perspective for the future study.

2. Model description

Following Serra et al. [13], let us consider a 1 m × 1 m square thin composite plate, as shown in Fig. 1, which comprises two plates of different masses but the same displacement from the overall center of mass (COM) $\boldsymbol{r}_{\text{com}}$.

In other words, the COM can be arbitrary. The dynamic system of this square thin plate has 13 state variables: the position and the velocity in the earth-centered inertial (ECI) frame, the attitude in quaternion form, and the rate of rotation in the body frame. The quaternions are used to avoid the singularity of the attitude. The governing equations consist of translational equations, Euler equations of motion, and attitude equations. The equations of translational motion read

$$\ddot{\boldsymbol{r}} = \left(\boldsymbol{a}_g + \boldsymbol{a}_a + \cdots\right), \tag{2}$$

where $\boldsymbol{a}_g$ denotes the acceleration due to gravity in the ECI frame, $\boldsymbol{a}_a$ is the acceleration due to atmospheric drag in the ECI frame, and so on. The acceleration due to gravity $\boldsymbol{a}_g$ is given by

$$\boldsymbol{a}_g = -\nabla U_E, \tag{3}$$

where U_E is the expansion of the geopotential in spherical harmonics. The spherical harmonic expansion coefficients with different accuracies correspond to different gravity field models. In this paper, the EGM96 gravity field model with 29 orders and degrees is adopted. The acceleration due to atmospheric drag is given by $\boldsymbol{a}_a$ is given by

$$\boldsymbol{a}_a = -\frac{1}{2} C_D \frac{S_{\text{ref}}}{m} \rho \|\boldsymbol{v}_{\text{rel}}\|^2 \frac{\boldsymbol{v}_{\text{rel}}}{\|\boldsymbol{v}_{\text{rel}}\|}, \tag{4}$$

where C_D is the drag coefficient, S_{ref} is the reference area of the plate, m is the mass of the plate, ρ is the atmospheric density, and $\boldsymbol{v}_{\text{rel}}$ is the relative velocity with respect to the atmosphere. Here, the atmospheric density ρ is calculated by the NRLMSISE-00 model [41], and the drag coefficient C_D is obtained by means of direct simulation Monte Carlo (DSMC) [42].

The attitude equations of the rotational motion read

$$\begin{cases} \dot{Q}_1 = \dfrac{1}{2}(-Q_4 p - Q_3 q + Q_2 r), \\ \dot{Q}_2 = \dfrac{1}{2}(Q_3 p - Q_4 q - Q_1 r), \\ \dot{Q}_3 = \dfrac{1}{2}(-Q_2 p + Q_1 q - Q_4 r), \\ \dot{Q}_4 = \dfrac{1}{2}(Q_1 p + Q_2 q + Q_3 r), \end{cases} \tag{5}$$

and the Euler equations of the rotational motion are

$$\begin{cases} \dot{p} = P_{pp} p^2 + P_{pq} pq + P_{pr} pr + P_{qq} q^2 + P_{qr} qr \\ \qquad + P_{rr} r^2 + P_x M_x + P_y M_y + P_z M_z, \\ \dot{q} = Q_{pp} p^2 + Q_{pq} pq + Q_{pr} pr + Q_{qq} q^2 + Q_{qr} qr \\ \qquad + Q_{rr} r^2 + Q_x M_x + Q_y M_y + Q_z M_z, \\ \dot{r} = R_{pp} p^2 + R_{pq} pq + R_{pr} pr + R_{qq} q^2 + R_{qr} qr \\ \qquad + R_{rr} r^2 + R_x M_x + R_y M_y + R_z M_z, \end{cases} \tag{6}$$

where Q_1, Q_2, Q_3, Q_4 are the quaternions that represent the attitudes of the plate, p, q, r are angular rates of rotation of the plate, M_x, M_y, M_z are the torques, and the definition of the coefficients can be found in reference [43], which are constants and relate to the moment of inertia. It should be noted that the quaternions are physically bounded in the range of $[-1, 1]$.

The target orbit is located at the LEO, where atmospheric drag is relatively large and thus the external forces are aerodynamics and gravity. Without loss of generality, let us consider the initial conditions listed in Table 1. The properties

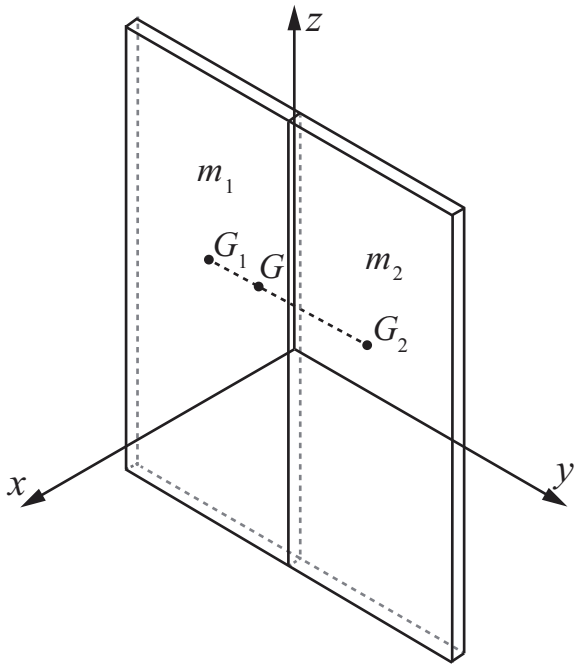

Figure 1 Schematic of the square plate, the COM G and the coordinate frame.

Table 1 Initial conditions of the plate in the LEO

Orbital elements	Value	Quaternions	Value	Angular rates	Value
Semimajor axis a (km)	7100	Q_1	0.0	p (rad/s)	0.01
Eccentricity e	0.001	Q_2	0.366	q (rad/s)	−0.02
Inclination i (deg)	89	Q_3	0.211	r (rad/s)	0.03
Perigee ω (deg)	30	Q_4	0.643		
Ascending node Ω (deg)	60				
True anomaly φ (deg)	100				

of the plate in two different cases are given in Table 2. For each case, we use two initial conditions: the original initial conditions and the initial conditions with a very small disturbance 10^{-12} at angular rate p. In this paper, the 8th-order Adam-Bashforth-Moulton (ABM) integration with the Bulirsh-Stoer method is used, with a time step 10^{-2} s.

3. Ultra-chaotic behavior of the square plate

3.1 Ultra-chaos

As discussed in Ref. [37], the statistical results of an ultra-chaotic system are susceptible to external small disturbances. In other words, the probability density functions (PDFs) of the variables in an ultra-chaotic system can vary as a result of small differences in initial conditions.

Through analysis of the trajectories of each of the variables from the different subsystems, it is found that both cases exhibit the properties of a chaotic system, since the error grows

Table 2 Properties of the plate in the LEO with different cases

Case	$\boldsymbol{r}_{\text{com}}$ (m)	m (kg)	m_1/m	$[\boldsymbol{I}_x, \boldsymbol{I}_y, \boldsymbol{I}_z]$ (kg · m^2)
A	[0.0, 0.075, 0.175]	0.1	0.62	$[1.61 \times 10^{-2}, 8.33 \times 10^{-3}, 2.08 \times 10^{-3}]$
B	[0.0, 0.120, 0.175]	0.1	0.74	$[1.52 \times 10^{-2}, 8.33 \times 10^{-3}, 2.08 \times 10^{-3}]$

exponentially and has a positive Lyapunov exponent. The Lyapunov exponents in case A and case B, as listed in Table 1 are 0.094 and 0.627, respectively. As an example, we demonstrate the normal-chaos and ultra-chaos of the square plate in LEO through two cases listed in Table 1 by means of the rotational subsystem.

Phase plot of the q and the $\dot{q}$ in case A of Table 1 are depicted in Fig. 2(a) and (b). Figure 2(a) displays the trajectory calculated with the undisturbed initial condition, while Fig. 2(b) shows the trajectory calculated with the undisturbed initial condition with a small disturbance. It can be observed that, despite the difference in initial conditions, the trajectories of the chaotic variable maintain the same structure. This difference in initial conditions is reflected in the magnitude of the error growth, but not in the structure of its trajectories. However, the situation in the chaotic system of case B in Table 1 differs from that of case A. The difference in initial conditions affects the structure of the trajectories in the phase space as demonstrated in Fig. 2(c) and (d). By definition, it can be concluded that the chaotic angular rate system of case A in Table 1 is characterized as normal-chaos, while the chaotic angular rate system of case B in Table 1 is characterized as ultra-chaos. Additionally, as illustrated in Fig. 3, the PDFs of q remain consistent under the tiny disturbance in the normal-chaos, while the PDFs of q are sensitive to the small disturbances and thus unstable in the ultra-chaos. Besides, ultra-chaotic behavior may stem from the interplay of nonlinearity, factors closely associated with integrability. As

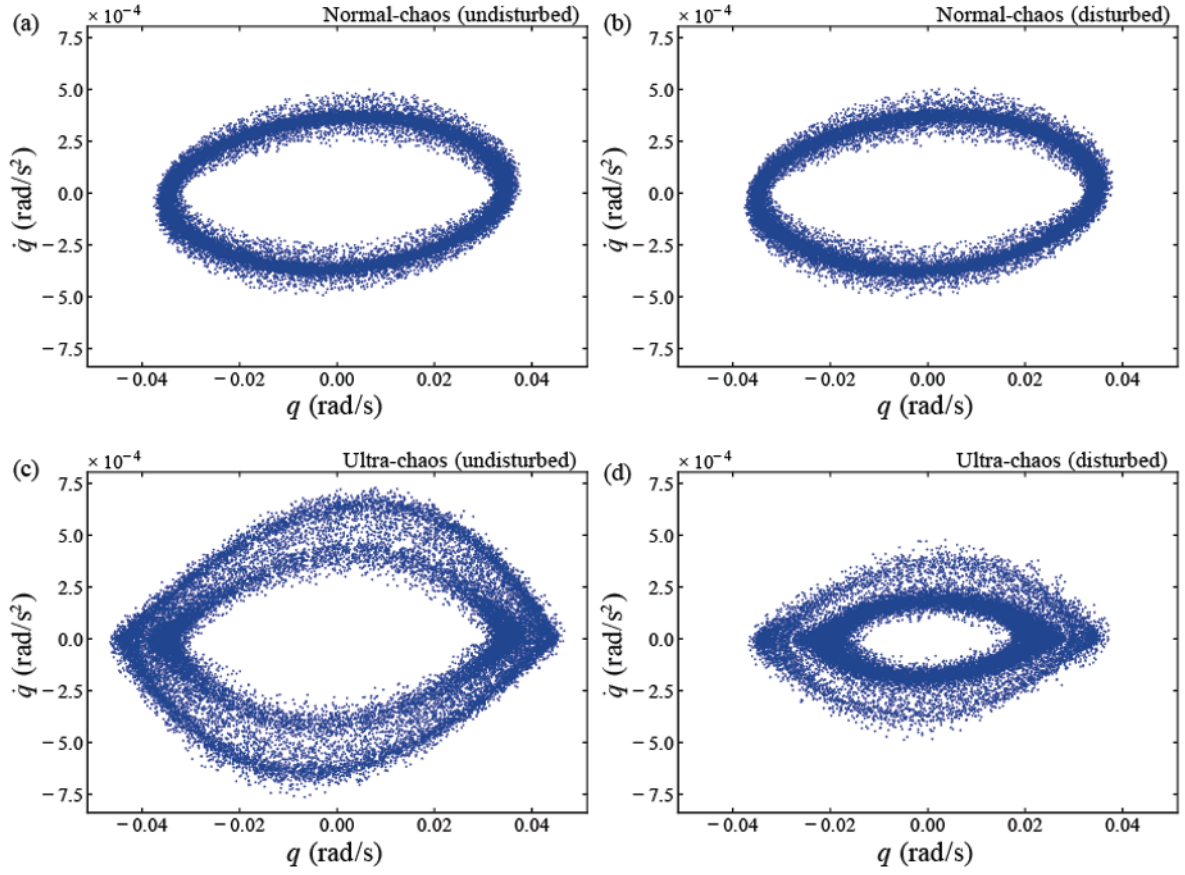

Figure 2 Influence of tiny disturbances on the q-$\dot{q}$ phase plot of a thin plate system. "Undisturbed" means the trajectory is calculated with the undisturbed initial condition, while "disturbed" means the trajectory is calculated with the undisturbed initial condition with additional tiny disturbance. (a) q-$\dot{q}$ phase plot for undisturbed initial condition which exhibits normal-chaos; (b) q-$\dot{q}$ phase plot for undisturbed initial condition with a tiny disturbance which exhibits normal-chaos; (c) q-$\dot{q}$ phase plot for undisturbed initial condition which exhibits ultra-chaos; (d) q-$\dot{q}$ phase plot for undisturbed initial condition with tiny disturbance which exhibits ultra-chaos.

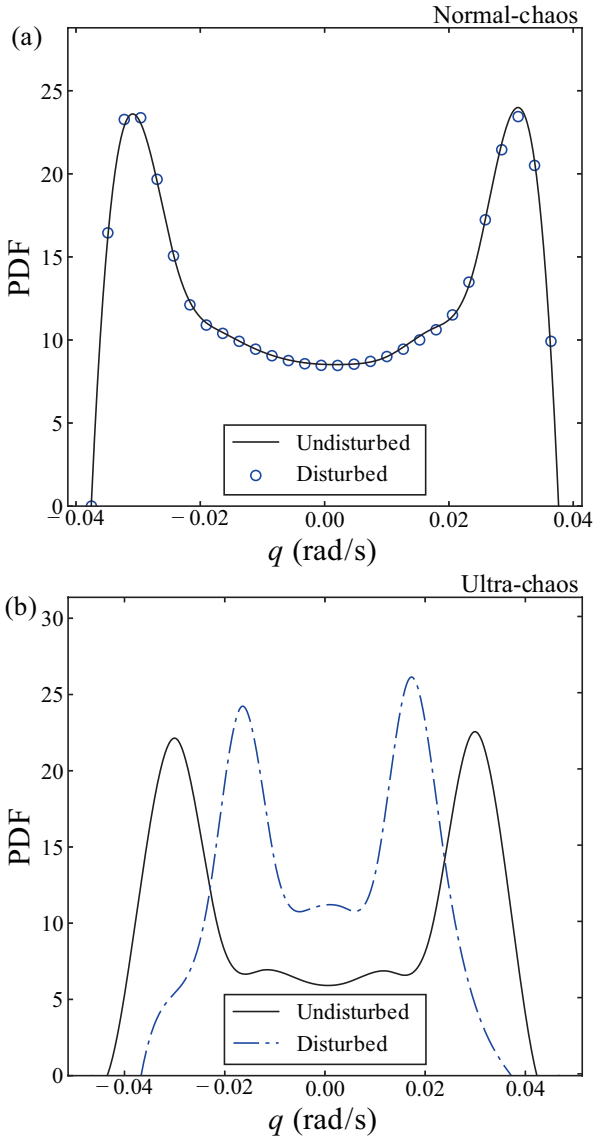

Figure 3 Influence of tiny disturbances on the PDFs of q. "Undisturbed" means the trajectory is calculated with the undisturbed initial condition, while "Disturbed" means the trajectory is calculated with the undisturbed initial condition with additional tiny disturbance. (a) PDFs of q of normal-chaos; (b) PDFs of q of ultra-chaos.

elucidated by Ma [44, 45], the precise equilibrium of coefficients, including both nonlinearity and dispersion, is essential for the preservation of integrability. The intricate connection between ultra-chaos and integrability remains a subject of ambiguity, warranting further in-depth investigation.

Furthermore, as demonstrated in Fig. 4, by varying the COM, i.e., values of y_{com} and z_{com} while keeping other physical parameters constant, it is found that ultra-chaos is a widespread phenomenon for the square thin plate system with a displaced COM from the axis of symmetry in the LEO. The mean value of the Lyapunov exponents within the normal-chaos regions is 0.47, while the mean Lyapunov exponent within the regions of the ultra-chaotic plate system

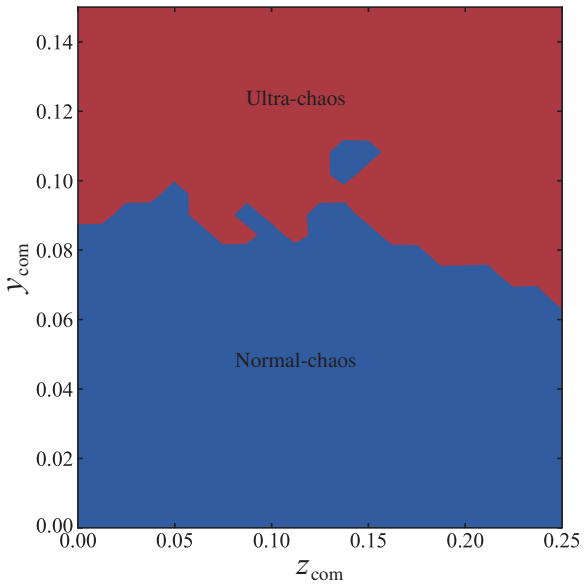

Figure 4 Phase plot of the plate system. Red domain: ultra-chaos; blue domain: normal-chaos.

is 0.10. The Lyapunov exponents of the ultra-chaotic plate system significantly exceed those of the normal-chaotic plate system, suggesting that the ultra-chaotic plate system exhibits a notably higher degree of disorder compared to the normal-chaotic plate system. It is worth noting that the boundary between ultra-chaos and normal-chaos is roughly plotted, and Fig. 4 only indicates the ubiquity of ultra-chaos. A finer grid could be employed to obtain a more precise boundary.

3.2 Influence of ultra-chaos on composite systems

According to our numerical experiments mentioned above, the statistics of the angular subsystem are stable in a normal-chaos, but unstable in an ultra-chaos. How does this statistic instability influence the whole system? The LEO system with 13 variables is a cyclic coupling system composed of three unidirectional coupling systems: the translational motion system S_t, the attitude system of the rotational motion system S_{r_1}, and the angular rate system of the rotational motion system S_{r_2}. We choose q, Q_2, and x to represent different subsystems of the square thin plate. The unidirectional coupling system consists of two parts: the driver and the response. In the system we discussed, the relationships among the three unidirectional coupling systems are as follows: in the unidirectional coupling between S_{r_1} and S_{r_2}, the S_{r_2} acts as the driver and the S_{r_1} acts as the response; in the unidirectional coupling between S_t and S_{r_1}, the S_{r_1} acts as the driver and the S_t acts as the response; in the unidirectional coupling between S_{r_2} and S_t, the S_t acts as the driver and the S_{r_2} acts as the response.

As shown in Fig. 5(a) and (b), the structures of the Q_2-$\dot{Q}_2$ phase plot remain unchanged in case A of Table 1. This is because the subsystem S_{r_2} with different initial conditions has the same PDFs, as shown in Fig. 6(a), due to the nature of the normal-chaos. On the contrary, The subsystem S_{r_2} in case B of Table 1 is an ultra-chaotic system and its small differences in initial conditions can have a significant impact on the PDFs of the trajectories in phase space. As demonstrated in Fig. 2, the angular rates in S_{r_2} can occupy different ranges of values, which then influence the response of S_{r_2}, i.e., the S_{r_1}. As shown in Fig. 5(c) and (d), the structures inside the trajectories of the S_{r_1} have changed, and its PDFs are also different in Fig. 6(b). This indicates that subsystem S_{r_1} is an ultra-chaotic system that is elicited by the ultra-chaotic behavior of subsystem S_{r_2}. Furthermore, this ultra-chaotic system possesses a physical boundary, as it involves variables that pertain to quaternions.

Ultra-chaos can transfer the initial error within the unidirectional coupling system of the whole system, and ultimately influence the S_t, as shown in Fig. 7. This is because the phase-space difference in trajectories of subsystem S_{r_2} alters the phase-space in subsystem S_{r_1}, leading to a different attitude PDF. These different attitudes further influence the subsystem S_t through aerodynamics, which governs the translational motion of the debris. The errors in position continue to accumulate, causing the trajectories of the plate to separate. Thus, a plate system that contains an ultra-chaotic subsystem will result in a significant error in the position of the plate. However, the initial difference in the angular rate of a plate system with a normal-chaotic subsystem spreads across the subsystems gradually, causing the error in the relative position to grow slowly, as shown in Fig. 7.

It is worth noting that the relative position error in case B of Table 1 is approximately two orders of magnitude larger than that in case A of Table 1. This is a non-negligible factor for predicting the trajectory of space debris that contains an ultra-chaos. Moreover, a satellite explosion will produce thousands of debris, the majority of which has a displaced

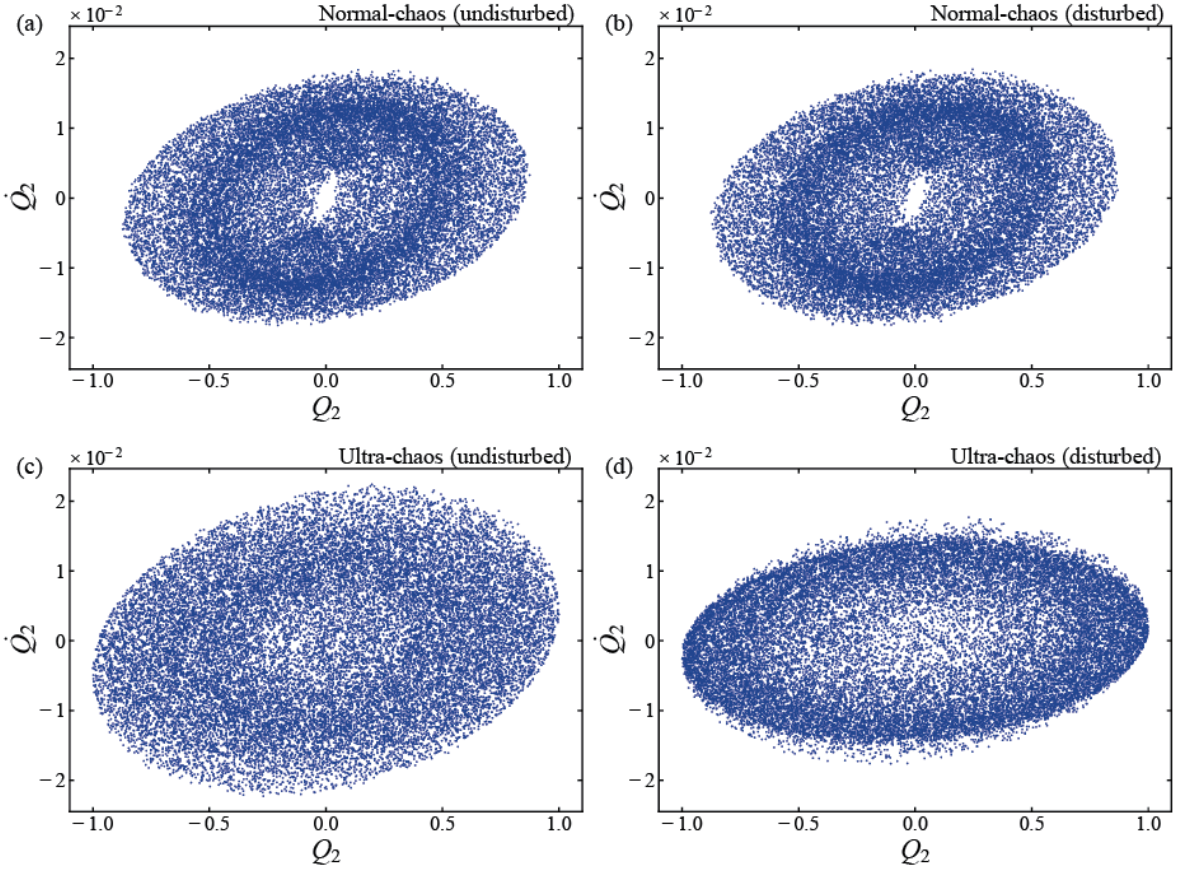

Figure 5 Influence of tiny disturbances on the Q_2-$\dot{Q}_2$ phase plot of a thin plate system. "Undisturbed" means the trajectory is calculated with the undisturbed initial condition, while "disturbed" means the trajectory is calculated with the undisturbed initial condition with additional tiny disturbance. (a) Q_2-$\dot{Q}_2$ phase plot for undisturbed initial condition which exhibits normal-chaos; (b) Q_2-$\dot{Q}_2$ phase plot for undisturbed initial condition with tiny disturbance which exhibits normal-chaos; (c) Q_2-$\dot{Q}_2$ phase plot for undisturbed initial condition which exhibits ultra-chaos; (d) Q_2-$\dot{Q}_2$ phase plot for undisturbed initial condition with tiny disturbance which exhibits ultra-chaos.

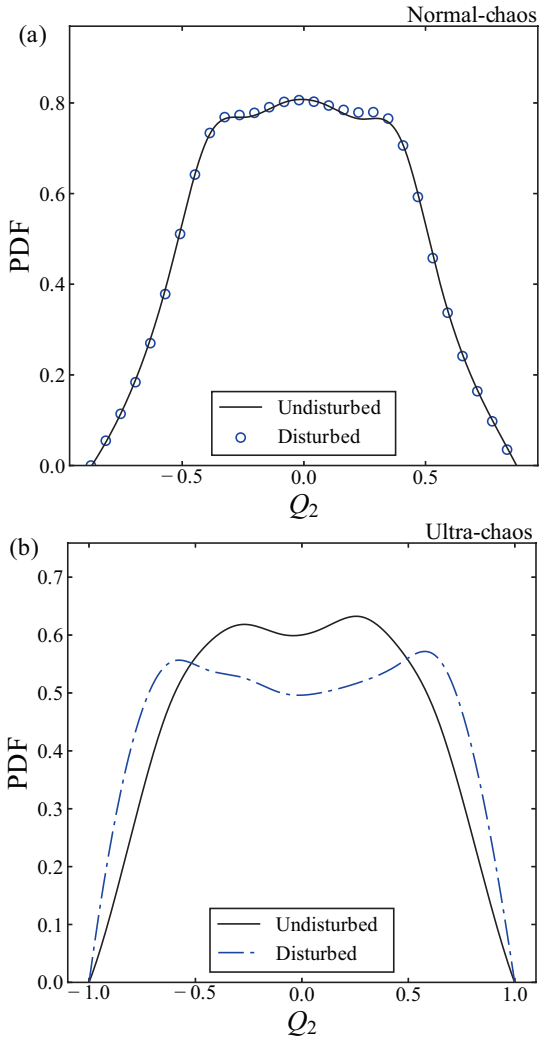

Figure 6 Influence of tiny disturbances on the PDFs of Q_2. "Undisturbed" means the trajectory is calculated with the undisturbed initial condition, while "disturbed" means the trajectory is calculated with the undisturbed initial condition with tiny disturbance. (a) PDFs of Q_2 of normal-chaos; (b) PDFs of Q_2 of ultra-chaos.

COM from the axis of symmetry. There is a high likelihood that the debris will form an ultra-chaotic system, which contributes to the extensive diffusion of the satellite explosion debris.

4. Conclusions

This paper has studied the behavior of a 13-variable chaotic thin square plate system in LEO. For the first time to the authors' knowledge, it is found that the chaos of the angular rate subsystem has two different types: normal-chaos and ultra-chaos. Unlike a normal-chaos system, the statistic results of an ultra-chaotic system are sensitive to small disturbances. It is found that the trajectory of an ultra-chaotic plate is in higher disorder than that of a normal-chaotic plate: the position deviation of the former can be two orders of magnitudes larger than the latter. The transfer of ultra-chaotic properties from the driver system to the subsequent coupling subsystem can have a significant impact on the trajectories of plates in LEO. The current study presents novel findings regarding ultra-chaotic systems, because the observed ultra-chaos occurs within a physically bounded system. This is in contrast to earlier investigations, which either featured at least one periodic boundary or lacked a physical boundary altogether. Ultra-chaos offers a plausible explanation as to why space debris can spread to a vast area, as most debris objects have a displaced centre of mass. At the time of writing, the LEO contains a large number of in-orbit debris objects of different shapes and sizes which are subject to various external forces, including third-body induction, solar radiation photovoltage, and Lorenz electromagnetic forces, which make it challenging to accurately predict the location of ultra-chaotic plate debris. To address this challenge, a feasible solution would be to correct the prediction results in real-time using observational data, also known as data assimilation (DA).

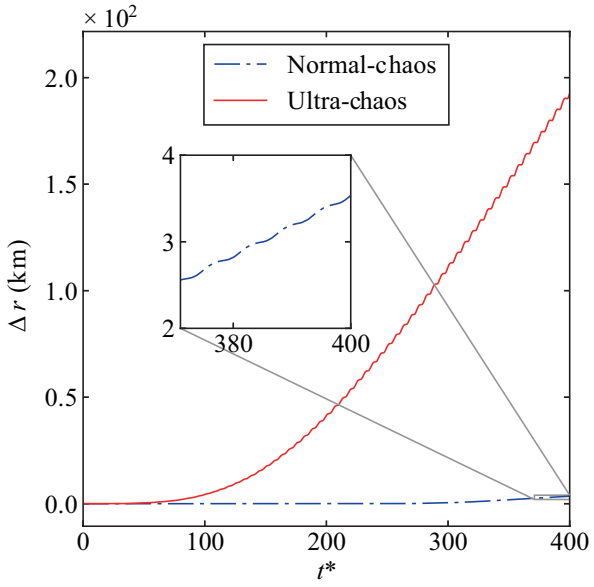

Figure 7 The temporal evolution of separation distance with different initial conditions in selected cases. The red line is the distance of ultra-chaos, while the blue dashdot line is the distance of normal-chaos. The non-dimensional time t^* is calculated by $t^* = \sqrt{\frac{\mathrm{GM}_E t^2}{a^3}}$, where GM_E is the gravitational parameter of the Earth, t is the dimensional time, and a is the semi-major axis of the orbit.

Conflict of interest *On behalf of all authors, the corresponding author states that there is no conflict of interest.*

Author contributions *Shijun Liao designed the research. Bo Zhang set up the experiment set-up and processed the experiment data. Bo Zhang wrote the first draft of the manuscript. Shijun Liao and Yu Yang helped organize the manuscript. Shijun Liao revised and edited the final version.*

Acknowledgements *This work was partly supported by the National Natural Science Foundation of China (Grant No. 12272230), Shanghai Pilot Program for Basic Research-Shanghai Jiao Tong University (Grant No. 21TQ1400202), and the project "Development of Large-scale Spacecraft Flight and Reentry Surveillance and Prediction System" of Manned Space Engineering Technology (2018-2014). We express our sincere thanks to the anonymous reviewers for their valuable comments and suggestions.*

1 ESA Space Debris Office, ESA's Annual Space Environment Report, Technical Report GEN-DB-LOG-00288-OPS-SD (ESA, 2022).
2 C. Pardini, and L. Anselmo, in Evolution of the debris cloud generated by the Fengyun-1C fragmentation event: Proceedings of the 20th International Symposium on Space Flight Dynamics, Annapolis, 2007.
3 N. L. Johnson, in Orbital debris: The growing threat to space operations: Proceedings of the 33rd Annual Guidance and Control Conferences, Breckenridge, 2010.
4 Y. Jiang, Debris cloud of India anti-satellite test to Microsat-R satellite, Heliyon **6**, e04692 (2020), arXiv: 2008.05142.
5 H. Klinkrad, B. Fritsche, T. Lips, and G. Koppenwallner, Re-entry prediction and on-ground risk estimation, in: Space Debris. Springer Praxis Books (Springer, Berlin, 2006).
6 G. C. Layek, An Introduction to Dynamical Systems and Chaos (Springer, New Delhi, 2015).
7 E. N. Lorenz, Deterministic nonperiodic flow, J. Atmos. Sci. **20**, 130 (1963).
8 R. N. Valani, and D. M. Paganin, Attractor-driven matter, Chaos-An Interdiscip. J. Nonlinear Sci. **33**, 2 (2023), arXiv: 2110.03776.
9 J. M. Ottino, The Kinematics of Mixing: Stretching, Chaos, and Transport (Cambridge University Press, Cambridge, 1989).
10 A. Celletti, C. Efthymiopoulos, F. Gachet, C. Galeş, and G. Pucacco, Dynamical models and the onset of chaos in space debris, Int. J. Non-Linear Mech. **90**, 147 (2017), arXiv: 1612.08849.
11 J. Daquin, A. J. Rosengren, E. M. Alessi, F. Deleflie, G. B. Valsecchi, and A. Rossi, The dynamical structure of the MEO region: Long-term stability, chaos, and transport, Celest. Mech. Dyn. Astr. **124**, 335 (2016), arXiv: 1507.06170.
12 V. S. Aslanov, Chaos behavior of space debris during tethered tow, J. Guidance Control Dyn. **39**, 2399 (2016).
13 R. Serra, K. Hoshi, M. Vasile, and H. Yamakawa, Study of Lorentz force on debris with high area-to-mass ratios, J. Guidance Control Dyn. **41**, 1675 (2018).
14 A. Khan, and S. Kumar, Study of chaos in chaotic satellite systems, Pramana **90**, 13 (2018).
15 V. S. Aslanov, and A. S. Ledkov, Chaotic motion of a reentry capsule during descent into the atmosphere, J. Guidance Control Dyn. **39**, 1834 (2016).
16 E. N. Lorenz, Computational chaos-a prelude to computational instability, Phys. D-Nonlinear Phenom. **35**, 299 (1989).
17 E. N. Lorenz, Computational periodicity as observed in a simple system, Tellus A-Dynamic Meteor. Oceanogr. **58**, 549 (2006).
18 J. Teixeira, C. A. Reynolds, and K. Judd, Time step sensitivity of nonlinear atmospheric models: Numerical convergence, truncation error growth, and ensemble design, J. Atmos. Sci. **64**, 175 (2007).
19 E. N. Lorenz, Reply to comment by L.-S. Yao and D. Hughes, Tellus A **60**, 806 (2008).
20 L. S. Yao, and D. Hughes, Comment on "Computational periodicity as observed in a simple system," by Edward N. Lorenz (2006a), Tellus A-Dyn. Meteor. Oceanogr. **60**, 803 (2022), arXiv: 0709.2150.
21 L. S. Yao, Computed chaos or numerical errors, Nonlinear Anal. Model. Control **15**, 109 (2010).
22 W. G. Hoover, and C. G. Hoover, Comparison of very smooth cell-model trajectories using five symplectic and two runge-kutta integrators, Comput. Methods Sci. Technol. **21**, 109 (2015).
23 Q. Yu, Y. Li, and X. Liu, On the extinction route of a stochastic population model under heteroclinic bifurcation, Acta Mech. Sin. **38**, 221333 (2022).
24 S. Fang, N. Padar, M. J. Mirzaei, S. Zhou, and W. H. Liao, Disturbance rejection and performance enhancement of perturbed tri-stable energy harvesters by adaptive finite-time disturbance observer, Acta Mech. Sin. **38**, 521535 (2022).
25 Z. B. Wang, L. Chen, and M. J. Ni, Numerical simulation of turbulent flow in FlowCube platform under a strong magnetic field, Acta Mech. Sin. **39**, 323143 (2023).
26 Q. Jin, and Y. Ren, Nonlinear size-dependent dynamic instability and local bifurcation of FG nanotubes transporting oscillatory fluids, Acta Mech. Sin. **38**, 521513 (2022).
27 Q. Lai, C. Lai, P. D. K. Kuate, C. Li, and S. He, Chaos in a simplest cyclic memristive neural network, Int. J. Bifurcation Chaos **32**, 2250042 (2022).
28 J. Choi, A. L. Shaw, I. S. Madjarov, X. Xie, R. Finkelstein, J. P. Covey, J. S. Cotler, D. K. Mark, H. Y. Huang, A. Kale, H. Pichler, F. G. S. L. Brandão, S. Choi, and M. Endres, Preparing random states and benchmarking with many-body quantum chaos, Nature **613**, 468 (2023), arXiv: 2103.03535.
29 Y. W. Zhao, J. W. Xia, and X. Lü, The variable separation solution, fractal and chaos in an extended coupled (2+1)-dimensional Burgers system, Nonlinear Dyn. **108**, 4195 (2022).
30 W. Alexan, M. Elkandoz, M. Mashaly, E. Azab, and A. Aboshousha, Color image encryption through chaos and KAA map, IEEE Access **11**, 11541 (2023).
31 S. He, D. Vignesh, L. Rondoni, and S. Banerjee, Chaos and multilayer attractors in asymmetric neural networks coupled with discrete fractional memristor, Neural Netw. **167**, 572 (2023).
32 S. Liao, On the reliability of computed chaotic solutions of non-linear differential equations, Tellus A-Dyn. Meteor. Oceanogr. **61**, 550 (2009), arXiv: 0901.2986.
33 S. J. Liao, Clean Numerical Simulation (CRC Press, New York, 2023).
34 Z. L. Lin, L. P. Wang, and S. J. Liao, On the origin of intrinsic randomness of Rayleigh-Bénard turbulence, Sci. China-Phys. Mech. Astron. **60**, 014712 (2017), arXiv: 1612.00120.
35 T. Hu, and S. Liao, On the risks of using double precision in numerical simulations of spatio-temporal chaos, J. Comput. Phys. **418**, 109629 (2020), arXiv: 1910.11976.
36 S. Qin, and S. Liao, Large-scale influence of numerical noises as artificial stochastic disturbances on a sustained turbulence, J. Fluid Mech. **948**, A7 (2022), arXiv: 2208.11487.
37 S. Liao, and S. Qin, Ultra-chaos: An insurmountable objective obstacle of reproducibility and replication, Adv. Appl. Math. Mech. **14**, 799 (2022).
38 Y. Yang, S. Qin, and S. Liao, Ultra-chaos of a mobile robot: A higher disorder than normal-chaos, Chaos Solitons Fractals **167**, 113037 (2023).
39 S. Qin, and S. Liao, A kind of Lagrangian chaotic property of the Arnold-Beltrami-Childress flow, J. Fluid Mech. **960**, A15 (2023), arXiv: 2204.14056.
40 B. Zhang, and S. Liao, Ultra-chaos in a meandering jet flow, Phy. D-Nonlinear Phenom. **455**, 133886 (2023).
41 J. M. Picone, A. E. Hedin, D. P. Drob, and A. C. Aikin, NRLMSISE-00 empirical model of the atmosphere: Statistical comparisons and scientific issues, J. Geophys. Res. **107**, 1468 (2002).

42 M. L. Vasile, E. Minisci, R. Serra, J. Beck, and I. Holbrough, in Analysis of the de-orbiting and re-entry of space objects with high area to mass ratio: Proceedings of the AIAA/AAS Astrodynamics Specialist Conference, Long Beach, 2016.
43 E. Mooij, The motion of a vehicle in a planetary atmosphere. Technical Report LR-768 (Delft University of Technology, Faculty of Aerospace Engineering, 1994).
44 W. X. Ma, Four-component integrable hierarchies of Hamiltonian equations with $(m + n + 2)$th-order Lax pairs, Theor. Math. Phys. **216**, 1180 (2023).
45 W. X. Ma, AKNS type reduced integrable bi-Hamiltonian hierarchies with four potentials, Appl. Math. Lett. **145**, 108775 (2023).

近地卫星轨道上方形薄板的超混沌

张博, 杨宇, 廖世俊

摘要 由于其小质量和偏心率, 近地卫星轨道上的碎片运动可能是混沌的. 本文所研究的在近地卫星轨道中偏质心的方形薄板是混沌的. 混沌系统以其对初始条件的敏感依赖而闻名, 但其统计特性通常对小扰动不敏感. 然而, 最近提出的一个名为超混沌的状态, 其统计量对小扰动也同样敏感. 本文表明, 超混沌广泛存在于近地卫星轨道上的偏质心方形薄板中. 结果显示, 超混沌的轨迹比正常混沌的轨迹更为混乱, 位置偏差可能比正常混沌大两个数量级. 与以往发现的超混沌系统不同, 本研究揭示了一个没有周期性边界的物理约束系统中的超混沌状态, 而遗忘的超混沌系统至少有一个周期边界或缺乏物理边界. 超混沌概念合理地解释了空间碎片可以扩散很大区域的原因, 因为大多数碎片是偏质心的.